Calibrating SoilGen2 for interglacial soil evolution in the Chinese Loess Plateau considering soil parameters and the effect of dust addition rhythm

Keerthika N. Ranathunga [a, b,*], Peter A. Finke [a], Qiuzhen Yin [b], Yanyan Yu [c]

[a] Department of Environment, Research group of soilscape genesis, Ghent University, Coupure links 653, B-9000 Ghent, Belgium

[b] Earth and Life Institute, Georges Lemaitre Center for Earth and Climate Research, Université Catholique de Louvain, Place Louis Pasteur 3, B-1348 Louvain-la-Neuve, Belgium

[c] Institute of Geology and Geophysics, Chinese Academy of Sciences (IGGCAS), 19, Beitucheng Xilu, Chaoyang District, Beijing 100029, China

* Corresponding author.

E-mail address: KeerthikaNirmani.Ranathunga@UGent.be (K.N. Ranathunga).

Abstract

To better understand interglacial paleosol development by quantifying the paleosol development processes on the Chinese Loess Plateau (CLP), we need a soil genesis model calibrated for long timescales. Here, we calibrate a process-based soil genesis model, SoilGen2, by confronting simulated and measured soil properties for the Holocene and MIS-13 paleosols formed in the CLP for various parameter settings. The calibration was made sequentially on three major soil process formulations, including decalcification, clay migration and soil organic carbon, which are represented by various process parameters. The order of the tuned parameters was based on sensitivity analyses performed previously on the loess in West European and the CLP. After the calibration of the intrinsic soil process parameters, the effect of uncertainty of dust deposition rate on calibration results was assessed. Our results show that the simulated soil properties are very sensitive to ten reconstructed dust deposition scenarios, reflecting the propagation of uncertainty of dust deposition in model simulations. Our results also show the equal importance of calibrating soil process parameters and defining correct external forcings in the future use of soil models. Our calibrated model allows interglacial soil simulation in the CLP over long timescales.

Keywords: SoilGen2 calibration; Soil parameters; Uncertainty; Dust deposition

1. Introduction:

The Quaternary loess-paleosol sequences on the Chinese Loess Plateau (CLP) are remarkable terrestrial archives for understanding the interglacial paleosol formation over the past 2.6 million years (Ma). Despite numerous paleosol-paleoclimate studies, research focusing on quantifying interglacial pedogenic processes in the CLP is rare (Finke et al., 2021). Quantitative expressions of the soil-forming processes and evolving soil properties allow a better understanding of the development of the soil (Stockmann, 2011). To explore and quantify paleosol-forming processes in the CLP, we need a soil development model calibrated for long time scales on the interglacial paleosols. Such model must consider changes in soil forming factors (Jenny, 1941) by using them as external forcing to modulate soil development processes, leading to simulate soil properties.

Process-based soil development models are useful tools to reconstruct or predict soil characteristics in the past and future over long-term spans. During soil development, texture, mineralogy, organic matter content and chemical properties change at different periods, such as annual, decadal, centennial and millennial. Therefore, if a model simulates for multi-millennium periods, soil properties such as soil texture, soil organic carbon and associated soil characteristics like the relations between h (hydraulic head), Θ (volumetric water content) and K (hydraulic conductivity) as well as cation exchange capacity (CEC) cannot be regarded as constants. Therefore, soil processes such as clay production by physical weathering, clay migration and the carbon cycle must be dynamically simulated. Here, we use the SoilGen2 model (Finke, 2012), as it is one of the few and most complete soil profile development models (Minasny et al., 2015).

To maximize the reliability of the model output, the model should be calibrated by adjusting process parameters to obtain an optimal match between measured and simulated soil data. The process parameters to be adjusted should first be identified in a preceding sensitivity analysis.

For SoilGen2, sensitivity analyses were done using the Morris' method (Morris, 1991) for clay migration in European soils (Finke et al., 2015) and for the C-cycle in both Chinese and European soils (Yu et al., 2013). These analyses resulted in a calibration order based on decreasing sensitivities of the involved parameters.

Soil formation is controlled by external forcings (boundary conditions to the model, e.g. climate change, tillage history) and initial conditions (properties of parent materials) (Jenny, 1941), which, however, are often associated with uncertainty in paleosol study. Therefore, it is useful to check the calibrated model with respect to its sensitivity to possible realizations of external forcings.

In the CLP, wind-blown dust is the parent material for the formation of interglacial paleosols. Various studies have described the role of dust addition on the pedogenesis in the CLP (e.g. Liu, 1985; Kukla and An, 1989; An et al., 1991; Porter, 2001; Guo et al., 2002; Maher, 2016). Pang and Huang (2006) found that soil formation differences between two regions (middle and middle-lower reaches of the Yellow River) are due to continuous dust deposition into soils. Another study by Li et al. (2019) also revealed the importance of influx of aeolian input as (added) parent material of soils, which plays a vital role in pedogenesis. These studies proved that continuous dust addition makes soil profiles grow in two directions (upward and downward). Huang et al. (2003) stressed that there is a need to understand dust accumulation and rates in Holocene soil formation in the CLP. Dust addition was maximal during glacial periods, but continued during soil-forming intervals, albeit at a lower rate, and the deposited dust may have been modified by post-depositional processes (e.g. pedogenesis during warm periods), forming accretionary interglacial paleosols (Kemp, 2001; Sun et al., 2010). Kohfeld and Harrison (2003) have stated uncertainty in the dust addition reconstructions during glacial-interglacial cycles. Therefore, it is of relevance that we examine the influence of the uncertainty of dust addition reconstruction on the paleosol development in a modeling context.

Thus, the overarching goal of this study is to calibrate the SoilGen2 model (Finke, 2012), a soil process-based soil development model, for the interglacial soils formed in the CLP. The specific research objectives of this study are (a) to calibrate three major soil process formulations, sequentially: decalcification, clay migration and soil organic carbon cycle represented by various process parameters, and (b) to investigate the sensitivity of soil development to different dust deposition scenarios.

2. Materials and methods

2.1 Study area and soil profiles

The study area, CLP, has a typical continental monsoon climate (warm and arid, semi-arid) and is characterized by cold and dry winters and warm and wet summers. From Northwest to Southeast, the mean annual temperature increases from 6-8 °C to 12-14 °C, and the mean annual precipitation increases from 150-300 mm to 800 mm, of which 60% occurs during July, August and September through summer monsoon rains. Thus, the Northwest is semi-arid and the Southeast is semi-humid (Maher, 2016).Vegetation types and distribution also follow the climate gradient from Northwest to Southeast with desert and steppe grading into forests.

Considering the spatial variation of climate on the CLP, three Holocene soil (S0) (the most recent soil profiles) were used for the $CaCO_3$ and Soil Organic Carbon (SOC) calibration, namely, Xifeng (mean annual precipitation 550 mm, mean annual temperature 8.7 °C), Taoyu in Qing'an county (507.3 mm, 10.4 °C) and Chenjiagou in Qishan county (623.8mm, 12 °C).

Holocene soils are influenced by ongoing and continuous dust addition with high amounts of calcium carbonate, limiting the clay migration in the soil. The semi-arid climate in the area is not favorable for clay transport. In addition, compared with the MIS13 paleosols, measurements indicate that the two Holocene soil profiles (Tables S1, S2) have no depth variations of the clay fraction (<2µm), and in Xifeng (Table S4) there are some significant changes of the clay fraction (ranging from 8 to 22 %). As clay migration during S0 is relatively weak, the S5-1 paleosol, formed during Marine Isotope Stage (MIS) 13 about 500,000 years ago, was used for the clay migration calibration as this paleosol shows strong eluviation and pedogenesis (An et al., 1987; Yin and Guo, 2008; Lu et al., 2018). The S5-1 paleosol from five profiles are used: Changwu (578 mm, 9.2 ˚C), Luochuan (600 mm, 9.2 ˚C), Weinan (645 mm, 13.6 ˚C), Chang'an (603 mm, 13.1 ˚C) and Wugong (650-750 mm, 12-14 ˚C) (figure1).

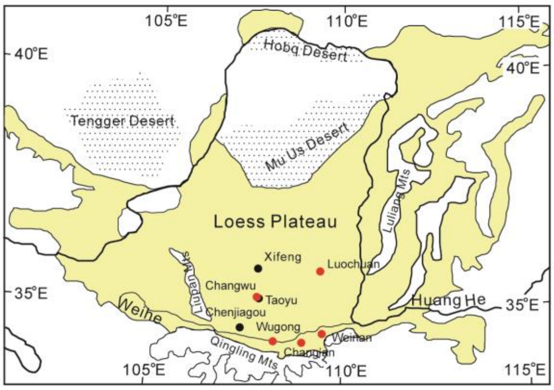

Figure 1. The locations of the soil profiles studied: black and red symbols represent the profiles used for S0 and for S5-1, respectively (modified after Hao and Guo (2005). The distribution of loess is indicated in yellow.

2.2 The SoilGen2 model

The SoilGen2 model (Finke and Hutson, 2008; Finke, 2012) is a one-dimensional (soil profile scale) model that can simulate vertical changes in soil properties over millenniums as result of pedogenetic processes driven by external forcings such as climate, vegetation and events like dust deposition. Below, we summarize its main functionalities.

The model simulates transport of water, heat and solutes by solving partial differential equations with finite differencing methods using the scheme of the LEACHC-model (Hutson and Wagenet, 1992). Plant uptake, decomposition of organic matter, fertilization, atmospheric deposition, erosion or sedimentation and precipitation, dissolution and adsorption of chemicals provide source and sink terms to these equations. Additionally, diffusive transport of CO_2 and vertical mass transport caused by bioturbation and plowing are simulated.

The soil development processes simulated by SoilGen2 include (de-)calcification and (de-)gypsification, physical weathering, chemical weathering of seventeen minerals, clay migration and the C-cycle.

Clay migration is simulated considering three main mechanisms: (i) splash detachment at the soil surface by raindrop impact, (ii) clay dispersion or flocculation in any soil compartment due to low or high ionic strength of rain or soil water, and (iii) filtering (Finke et al., 2015).

SoilGen2 simulates the five soil organic carbon (SOC) pools of the RothC 26.3 (Coleman and Jenkinson, 2014) model for each soil compartment. Decomposable plant material (DPM), resistant plant material (RPM), humified organic matter (HUM) and microbial biomass (BIO) degrade according a first-order process with specific decay rate constants modified by temperature and soil moisture. Decayed BIO and HUM partially recombine to mimic a food web. Inert organic matter (IOM) refers to an inactive (non-decaying pool) soil carbon pool. Carbon (C) cycle parameters are vegetation related. SoilGen2 distinguishes four vegetation:

grass/shrubland, deciduous and coniferous forest and agriculture. Each vegetation type has an input rooting depth, ion uptake forcing function, and parameters related to C-cycling (e.g. decomposition rates and the partitioning of plant litter to above and below ground).

The (1-D) model handles geomorphic processes such as erosion and sedimentation as events at the upper boundary by removing and adding soil layers. Agricultural practices are characterized by input fertilization, planting and harvesting dates and tillage. A simulated soil profile is discretized by multiple layers of equal thickness (e.g. 5 cm). The model simulation time steps vary with the simulated processes: for water and solute flow: seconds to hours, physical weathering and heat flow: every hour, SOC cycling and weathering: every day and bioturbation, erosion, and deposition: every year (figure 2). Thus, soil properties are generated by dynamic interactions between soil solid (mineral and organic matter), liquid and air phase. For detailed model description, reference is made to Finke and Hutson (2008), Finke (2012), Finke et al. (2015), Opolot et al. (2015) and Finke (2020).

The model has been tested for the above mentioned soil processes in several case studies, including the CLP. Here we elaborate these examples and its conclusions.

1. Carbon cycling process in the SoilGen2 model was calibrated for both Belgian and Chinese loess soils (Yu et al., 2013). Results showed that the decomposition rates k_{HUM} of humus and k_{RPM}, of resistant plant material, and the fraction of litter that is ectorganic, frecto, (leaf litter; (Kononova, 1975), were the most sensitive parameters. In addition, their calibration results were comparable to those obtained in previous studies. These results confirmed that the SoilGen2 carbon module can be applied to paleosols formed in the loess parent material.

2. The model has also been applied and tested for soil development in southern Norwegian soils (Sauer et al., 2012). They compared simulated soil properties with measured data from twelve soil profiles composing two soil chronosequences. Results showed that SoilGen2

simulated clay content, particle size distribution well, but underestimated soil properties such as CEC, organic carbon, base saturation and pH.

3. The clay migration module in the SoilGen2 model has been calibrated in French loess soils, by adapting six parameters (Finke et al., 2015). The calibrated model has been tested on a total of eighteen soil profiles, including both forest and agricultural soils. The results indicated that the h-θ_{macro} (the pressure head at which macropores empty) and the filter coefficient (n), were the most sensitive parameters.

4. A modeling study shows that SoilGen2 simulated soil properties could be sensitive to reconstructed boundary and initial conditions (Keyvanshokouhi et al., 2016) and these authors have documented SoilGen2 as a soil development model suitable for global change studies. Several authors have concurred on this point (Minasny et al., 2015; Kuzyakov and Zamanian, 2019). Moreover, Opolot et al. (2015) provide an extensive review of the SoilGen2 governing processes, integrating case studies mentioned. Therefore, the existing SoilGen2 model provides a fair opportunity for modeling soils and paleosols.

In the SoilGen2 model, the input data of initial and boundary conditions represent the major soil-forming factors (Climate, Organisms, Relief, Parent material):

- Climate is characterized by simulated time series of precipitation, potential evapotranspiration and temperature by the climate model LOVECLIM for the entire simulation period, which is essential for interglacial paleosol simulations (Yin and Berger, 2015). The simulated precipitation, potential evapotranspiration and temperature greatly differ between MIS1 and MIS13 (Figures S15.a, S15.b). Hereto, a typical daily series for one year is adapted to reflect monthly climate data simulated by LOVECLIM. We use multiplication factors (for precipitation and evapotranspiration) and differences (for temperature shifts), to match LOVECLIM data to SoilGen2. In this way, monthly sums (precipitation, evapotranspiration) or averages (temperatures) that are simulated using LOVECLIM are translated to SoilGen2 by monthly corrections. The simulated climate is downscaled to the location of interest (protocol in Finke et al., 2017, SI).

- The most probable vegetation for every year is obtained by downscaling the vegetation distribution over the CLP that was simulated by LOVECLIM to the location of interest.
- Starting date of agriculture for S0 is based on archeological data (Yu et al., 2016). Bioturbation and plant litter input were based on vegetation type and climate.
- For relief we assume a plateau position.
- The properties of the loess deposited in the preceding glacial period serve as initial conditions at the start of simulations, while the properties of the loess deposited during the interglacial are defined by those of the overlying loess. We assume that those loess properties remain the same for both under and -over lying loess. A detailed description of these inputs is presented in the supplementary information. (Tables S1, S2, S3, S5, S6, S12).

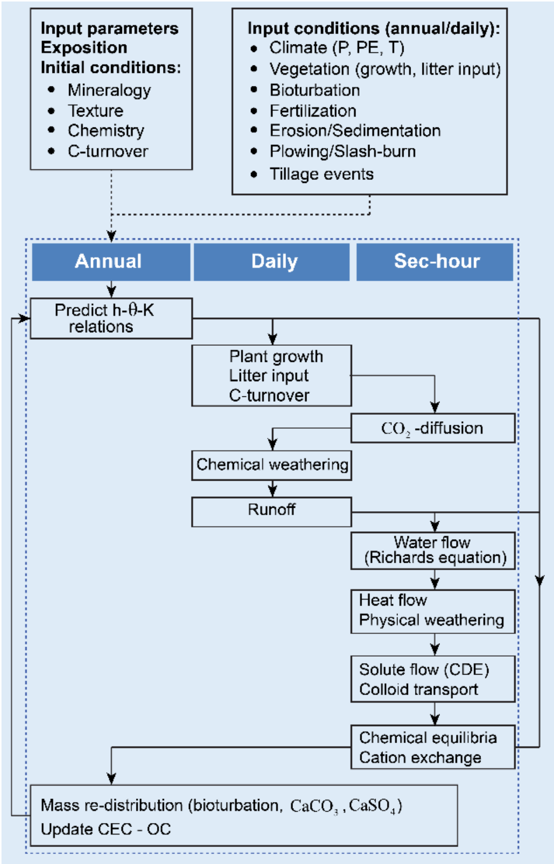

Figure 2. Soil process sequence in the SoilGen2 model, indicating input data at the upper boundary. Copied and adapted from Minasny et al. (2015). P, PE and T stand for precipitation, evaporation, temperature, respectively and CDE and CEC denote Convection Dispersion Equation and Cation Exchange Capacity accordingly. h-Θ-K denote the relations between hydraulic head, water content and hydraulic conductivity.

3. Model calibration and parameters

3.1 Calibration layout

We aim to obtain one set of calibrated parameters that are suitable for interglacial paleosol simulations in the loess plateau. As already mentioned, the calibration of soil process parameters was done partly for Holocene soils and partly for the S5-1 paleosol. Zwertvaegher et al. (2013) showed that soil could develop before the typical Holocene epoch (the past ~12ka BP) in Europe. Even though Holocene soil formation periods in the CLP are not consistent with Europe, our simulation periods are slightly longer than the Holocene, and they are 17-0 ka for the Holocene. It was done solely to include the less intensive soil formation periods during SoilGen2 simulations. Our choice will not affect the degree of soil development because, if the climate is cold or dry, leaching will not occur and no decalcification, clay migration will be simulated either. We simulate S5-1 paleosol for the period of 511-481 kyr. The calibration was done per group of process parameters in a predefined order. The order of the tuned parameters was based on published sensitivity analyses and feedback mechanisms in the soil. For instance, since clay migration hardly occurs in calcareous soils, it is necessary to calibrate (de-)calcification first and thereafter clay migration. Lastly, C-cycling parameters were calibrated. Therefore, these three main soil process formulations were calibrated representing various process parameters (table 1) (see sections 3.2, 3.3, and 3.4).

The optimal value for a parameter was selected using the dissimilarity (Gower, 1971):

$$DIS_{Profile} = \frac{1}{K}\sum_{k=1}^{K} abs\left(X_{r,k} - X_{s,k}\right) \qquad \text{[Eq.1]}$$

where X represents the soil property of interest, k is the number of soil compartments (55 in the present study); s refers to the value for the simulation and r for the reference (measurement).

Process parameters were adjusted until the average value for DIS reached a minimum over the locations of interest. During the calibration process, only the calibrating process parameter was changed (in the value range) while the others kept their average (initial) or previously calibrated values. As model runtime for simulations covering the Holocene or MIS13 are long (ca. 5 CPU-days per run), advanced calibration methods involving many simulations were unfeasible.

3.2 Decalcification

Calcium carbonate (calcite) content is a major soil property, noticeably in the arid and semi-arid CLP, and it is one of the major minerals (10-20%) in the loess when deposited (Liu, 1985). Decalcification or, more general, calcite redistribution, is a major soil-forming process in the loess plateau. It influences various soil properties e.g. soil pH, bulk density, porosity, cations in soil solution and determines differences in water storage between loess/paleosol layers due to changes in soil physical properties. In the SoilGen2 model, calcite redistribution is determined by the solubility of calcite and the transport of the solute (leaching). The solubility is defined by the $\log_{10}$kso (calcium carbonate dissolution constant), which was calibrated by analyzing results at eight equidistant values (table 1).

To calibrate the degree of leaching in soils, we calibrated the interception evaporation fraction. Only the effective rainfall of the total precipitation reaches the soil, via stem flow and throughfall, and the remaining water in the foliage (e.g. leaves, twigs, small branches) evaporates to the atmosphere during and after rain, as the fraction of net precipitation (Savenije, 2004; Li et al., 2016). Interception evaporation affects infiltration and thus solute transport into the deeper parts of the soil profile. The amount of intercepted water (vegetation dependent) was varied using seven equidistant values (ranging from 1% to 7%) for both grass/shrubs and agriculture (table 1).

3.3 Clay migration

Clay migration indicates the strength of pedogenesis and is a profile formation process. Clay migration can form a distinct clay-enriched layer over thousands of years (Van Breemen and Buurman, 2002). Clay migration was calibrated taking into account (1) splash detachment, (2) determination of the fraction of dispersible clay, (3) transport via macropores, (4) filtering and (5) production of clay by physical weathering. In the CLP, clay migration mainly starts after decalcification, when the double layer has lost Ca^{+2} ions by leaching (Vidic and Lobnik, 1997). Clay particles (<2μm) may accumulate at depth as a consequence of filtering or of flocculation (e.g. on top of a calcic horizon where the Ca^{+2} ions are abundant, Schaetzl and Thompson (2015). From an ecological point of view, the clay fraction is an important soil property for soil water retention and permeability characteristics in loess and paleosol sections. The parameters related to clay migration were calibrated after decarbonation.

The clay migration process was calibrated by tuning 4 individual processes (iii, iv, v, and vi in table 1). We first calibrate the ectorganic layer thickness (above ground leaf litter), as it reduces splash detachment of clay by limiting raindrops collisions with the mineral topsoil (see equation 11 in Finke, 2012). The role of the surface litter layer thickness has long been studied under different vegetation types in the loess plateau of China concerning soil erosion control, runoff and sediment accumulation (Li and Shao, 2006; Geißler et al., 2012; Zhou et al., 2016).

After that, the pressure head (h) at which soil macropores empty was calibrated. This allows to asses during simulation, via h, the amount of clay in contact with soil macropores. This clay, if in dispersed state, can be transported (see equation 14 in Finke, 2012).

During clay migration, some of the dispersed clay is filtered due to too low water flow velocities in macropores (Jarvis et al., 1999; DeNovio et al., 2004). The filter coefficient (n) was subjected to calibration (see equation 15 in Finke, 2012).

Lastly, two parameters that describe the rate of physical weathering as a function of soil temperature change were calibrated. PS_{max} is the maximal probability that soil particles split by physical weathering, and B is the temperature change (°C h^{-1}) at which the splitting probability becomes maximal. By updating the splitting probability as a function of temperature change, the model produces grains in the clay fraction. PS_{max} and B were calibrated concomitantly (16 pairs of values for B and PS_{max}).

The order of calibration of the clay migration parameters was based on a sensitivity analysis for West European loess soils, in a much moister climate than the CLP-climate (Finke et al., 2015).

Equations that describe physical weathering and clay migration-related parameters in the SoilGen2 model have been illustrated in section 2.2 in Finke (2012), supplementary information for Finke et al. (2015), sections 2.1.2.1 and 2.1.3 in Opolot et al. (2015), and Finke (2020).

3.4 Soil organic carbon

SOC influences various soil properties e.g. CEC, pH, porosity, bulk density; these also change during soil development. Variations in soil texture, temperature and moisture alter soil organic matter decomposition rates, which in turn can affect the SOC pools in soils.

Following the RothC 26.3 concepts, the turnover rate of organic matter added to the soil is described as follows; Eq. [2] depicts the amount of organic carbon (Y) that decomposes from active pools per month. Eq. [2] exponentially calculates the remainder of soil carbon at the end of each month.

$$Y = Y_0 \left(1 - e^{-abckt}\right) \qquad \text{[Eq. 2]}$$

Where, Y_0 is the starting amount of carbon from any active pool, *a* and *b* are the rate modifying factors for temperature and soil moisture respectively, *c* is the modifying factor for soil cover, *k* stands for decay rate constant for a particular pool, and *t* converts the annual decomposition rate constants into monthly values (t=1/12). Amongst these rate modifying factors, contributions per soil layer to the soil moisture deficit and temperature fluctuations vary over time and soil depth (in each 5 cm) in the model. Soil moisture deficit is defined as precipitation minus potential evapotranspiration, which deficit is distributed over depth using the air-filled porosity (soil water content minus porosity).

We followed the sensitive parameters identified by Yu et al. (2013), and added the slightly less sensitive partitioning coefficient CO_2 / (BIO+HUM), describing the fate of the lost C from BIO and HUM during decomposition. This partitioning coefficient is a function of soil clay content [Eq.3]:

$$\frac{CO2}{(BIO+HUM)} = 1.67\ (1.85 + 1.60\ e^{-0.0786*\%\ Clay}) \qquad \text{[Eq.3]}$$

Therefore, the order of SOC calibration was k_{HUM}, fr_{ecto}, k_{RPM} and finally the partitioning coefficient CO_2 / (BIO+HUM). For fr_{ecto}, only two Holocene sites were calibrated that had no agriculture.

Table 1. Calibrated parameters, value range and number of simulations.

Soil forming process	Order	Process parameter with units	Range of values	Simulations per parameter and total
(de)calcification	(i)	Dissolution constant of calcite (log_{10} k_{so})	-9.2 to -7.8	8 and 24
	(ii)	Interception evaporation fraction (-) for grass/shrubs/agriculture	0.01-0.07	7 and 21
Clay migration	(iii)	Thickness of the ectorganic layer (mm)	0.5-3.5	7 and 35
	(iv)	Pressure head (hPa) at which macropores empty	-6 to -30	7 and 35
	(v)	Filter coefficient for clay (-)	0.2-0.8	7 and 35
Physical weathering	(vi)	Particle splitting probability (PS)	1.338×10^{-6}-2.163×10^{-6}	16 and 80
		soil temperature change (B) °C / hour (4x4 combinations)	0.45-1.95	
Organic carbon cycle	(vii)	Decomposition rate (yr^{-1}) of humus	0.001-0.035	12 and 36
	(viii)	Ratio of ectorganic/endorganic litter (-)	0.35-0.7	11 and 22
	(ix)	Decomposition rate of (yr^{-1}) of resistant plant material	0.01-0.675	13 and 39

(x)	Partitioning coefficient CO_2 / (BIO+HUM)	0.3-3.0	9 and 27

3.5 The uncertainty of dust deposition rhythms on soil development

Changing dust addition speed over time can influence the rates of soil processes. For instance, lower speed allows more time for calcite leaching, whereas higher speed rapidly re-carbonates the soil. Therefore, we explored the uncertainty of dust addition on the calibration results.

Hereto, ten Holocene dust deposition scenarios were applied to determine whether the calibrated results are persistent in this respect. Here, we solely considered the variation of the speed of dust addition over time (rhythm for short) while assuming that the mineralogical composition of the added dust as well as the total amount of added dust remain similar. Dust accumulation rhythms were reconstructed in various case studies (references in Table S14) using depth-age models. However, there were depositional hiatuses in the published dust records due to uncertainty of soil age. We recovered those distorted age points by linear interpolation between the more certain ages in the original series. Albani et al. (2015) reported that this method has uncertainties depending on the used age points. Dust addition was mimicked by adding compartments of 5 cm during soil development. Each year when the added dust thickness reaches a multifold of 5 cm was used to add 1 compartment. In general, the selected dust records exhibit higher dust addition during both the early and/or the late Holocene relative to the middle Holocene (figure 3).

We analyzed the effect of ten reconstructed dust deposition scenarios on the simulated soil properties calcite, organic carbon, 2µm fraction and CEC. To compare the soil properties, we applied scaled dissimilarity, the ratio between the unscaled dissimilarity (DIS) (see Eq. [1]), and the difference of maximum and minimum measured value of the corresponding soil property in that particular profile. The scaled dissimilarity is dimensionless, and thus soil variables can be compared.

We compared the scaled dissimilarity of the best calibration with those of the dust scenarios, and compared the impact of these dust scenarios to the quality of the calibrations by calculating a standard deviation for each considered soil property:

$$sdDIS_{scaled} = \sqrt{\frac{1}{10} \quad \sum_{i=1}^{10}(DIS_{scaled,i} - DIS_{scaled,cal})^2} \qquad \text{[Eq.4]}$$

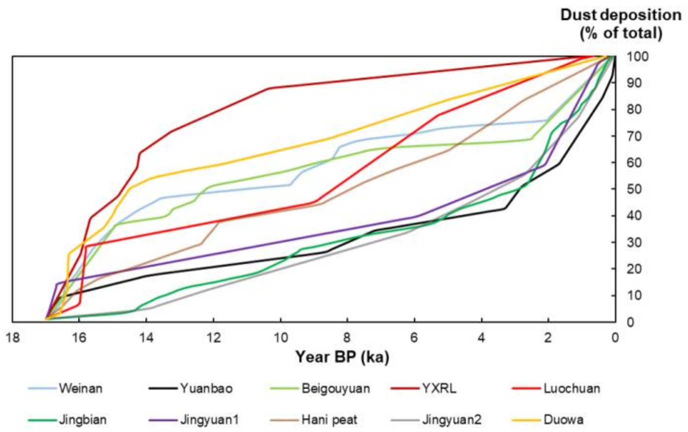

Figure 3. Ten dust deposition rhythms applied in SoilGen2.

4. Results and Discussion

4.1 Decalcification

The best-calibrated $\log_{10}$kso (lowest averaged dissimilarity) was -9.0 for the studied three profiles (figure 4.A). This result was in between the previous values for $\log_{10}$kso: –9.2 (Zwertvaegher et al., 2013), -8.46 for Belgium and Hungary loess soils (Finke and Hutson, 2008) and -8.36 for Belgium loess soils (Finke, 2012), which were typically derived for European loess soils, leaching climate, whereas CLP possesses a semi-arid climate. Laboratory experiments have found $\log_{10}$kso -8.48 at 25 °C (Jacobson and Langmuir, 1974).

The $\log_{10}$kso of -9.0 indicates a low dissolution rate of calcite. This may be caused by (i) the temperature correction to the solubility constant (different temperature regimes in Europe and the CLP), (ii) the grain sizes of the calcite, and (iii) the lower leaching in the semi-arid CLP (Li et al., 2013; Li et al., 2018).

The best-calibrated interception loss for grass/shrub and agriculture was 3% (figure 4.B). We assumed an equal amount of interception loss for all types of vegetation dominating in the Holocene at the sites of interest: grass/shrubs and agricultural crops. This interception loss was much lower for shrublands than the literature reported (table S13). Ochoa-Sánchez et al. (2018) has reported interception values for grasses (in there table 2) from the global literature, where the grass interception loss is between maximum 100% - minimum 5% of the total precipitation. The calibrated interception loss approximately fits at the lower end of the literature findings, and for agricultural crops, it closes to the values reported by Wang et al. (2012) (see table S13).

The interception loss varied between forest types: we assigned 14% for deciduous and 21% for coniferous. These values corresponded to 175% of the SoilGen2 model default (deciduous=8% and coniferous=12%). Varying these percentages did not affect decalcification, since Holocene soils were not covered by forests for long periods at the studied locations, whereas grasses/scrubs and agriculture were the dominating vegetation types (Yu et al., 2016; Sun et al., 2017). The forest interception losses (14% and 21%) are well comparable to Su et al. (2016)'s findings (14.3% for broadleaved forests), and between 14.7%-31.8% (Wei et al., 2005) for major Chinese forests and within the range of 11.1% and 24% (Liu et al., 2003; Zhang et al., 2006; Wang et al., 2012; Jian et al., 2015; Sheng and Cai, 2019) (see table S13).

In general, calibrated canopy interception losses were consistent with other authors' findings and statements (e.g. Nisbet, 2005), who stated that forests intercept more than grasslands because grass/shrubs or crops have less canopy than forests. Thus, our results were not unexpected. Moreover, these results agree with values reported for forest canopy interception. This interception can take up an amount of 10-50% of total rainfall (Klaassen et al., 1998; Carlyle-Moses and Gash, 2011), in which coniferous takes 25-50%, and broadleaved occupies 10-35% (Rutter et al., 1975), and it is about 12-25% in semi-arid areas (Hörmann et al., 1996).

The high variation of interception found in literature can be attributed to various factors: Climate (rainfall variability, intensity and duration) as well as vegetation characteristics (species, canopy storage capacity, plant morphological and biomass-related traits of species: e.g. tree density, leaf area index, leaf shape, canopy structure) (Hörmann et al., 1996; Crockford and Richardson, 2000) are not easily measured. Therefore, we assume that the calibrated interception losses are fair.

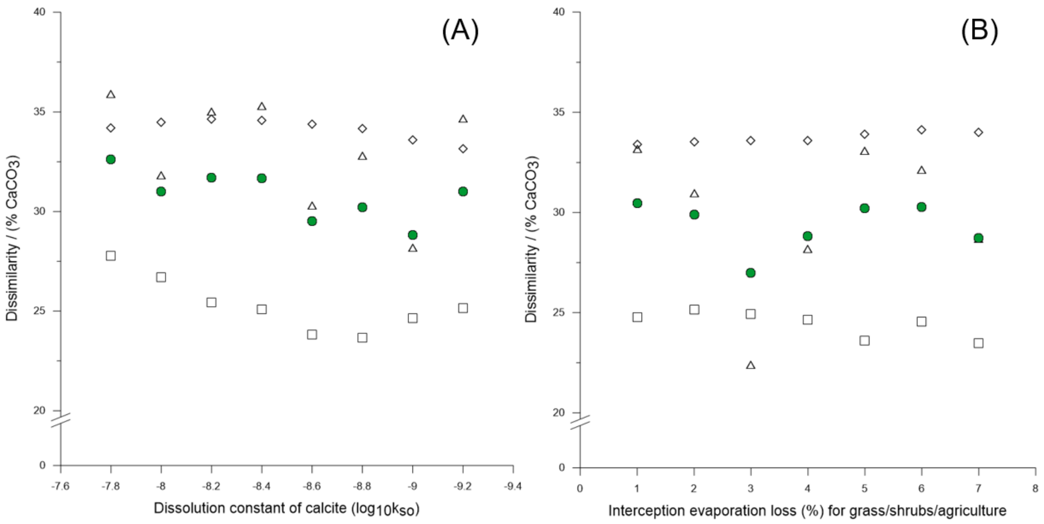

Figure 4. Dissimilarity (%) as a function of (A).the calcite dissolution constant ($\log_{10}k_{so}$) and (B). the interception evaporation loss (%) for grass/shrubs/agriculture in three profiles: Xifeng, Chenjiagou, Taoyu are denoted by open triangles, diamonds, squares, respectively. Green dots show profile averages.

4.2 Clay migration

Results showed unexpected indifference of clay migration to the pressure head at which macropores empty (h-θ_{macro}) (figure 5.A). We confirmed this result by evaluation of various additional h-θ_{macro}. The reason for this may be the drier climate in semi-arid China, which causes most macropores to be air-filled and consequently macropore water flow velocity and associated clay transport will be less, which will increase filtering. DeNovio et al. (2004) also emphasized the importance of pore water velocity on clay migration. Until now, the pressure head h-θ_{macro} had been calibrated for leaching climates in Western Europe, e.g. -1hPa (Finke, 2012) and -18.3hPa (Finke et al., 2015). These studies have confirmed that the clay translocation depths of the soils are highly dependent on h-θ_{macro} and the filter coefficient (n). Thus, we conclude that the amount of precipitation is the critical and limiting climate variable that determines clay migration in arid and semi-arid Chinese loess regions. Therefore, the initial value of -18hPa was kept in the following steps.

The filter coefficient (n) also determines the clay mobility in the soil. The best-calibrated "n" was 0.5 at the minimum dissimilarity (figure 5.B), which was comparable with previous calibrated results: 0.6607 (Finke, 2012) for loess soils in Belgium, 0.51 (Finke et al., 2015) for loess-derived soil in northern France and 0.7 for silt-clay soils in Sweden (Jarvis et al., 1999).

Regarding physical weathering, optimal-calibrated values were found for PS_{max} at 2.163 x 10^{-6} and B at 0.95 °C / hour across five soil profiles (figure 5.C). Finke et al. (2015) found the PS_{max} and B at 1.338 x 10^{-6} and 1.95 °C / hour respectively in French soils, and Finke (2012) obtained best-calibrated results at 3 x 10^{-6} for PS_{max} at 1° C / hour soil temperature gradient. The calibrated PS_{max} in this study was in between the PS_{max} of these studies and is plausible.

Concerning the ectorganic layer thickness, the best-calibrated value was 0.5 mm (figure 5.D). We could not refer to literature because no studies refer to this parameter in the context of modeling. Finally, a check showed that the ectorganic layer thickness variations did not change the indifference to the pressure head h-θ_{macro}.

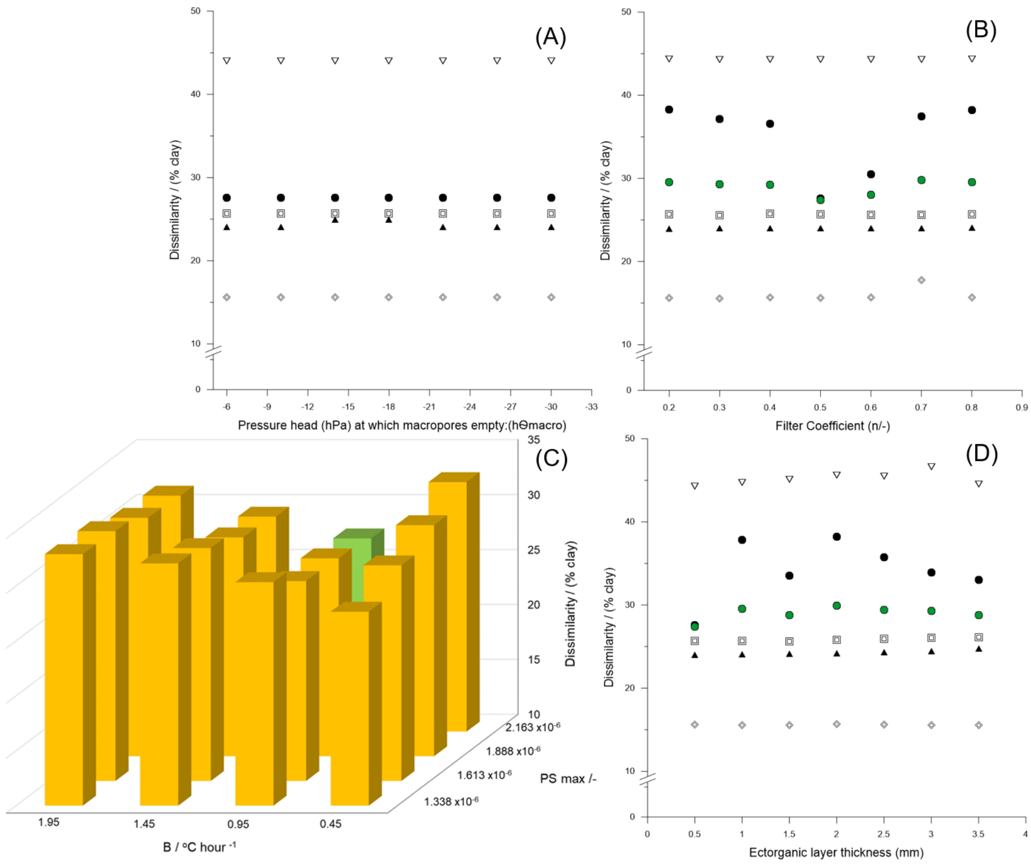

Figure 5. Dissimilarity (%) as a function of (A). pressure head h-θ_{macro} (hPa), (B). filter coefficient n(-), (C). PS_{max}-B combinations. Green bar shows the best average for five profiles. (D). ectorganic layer thickness (mm) in five profiles: symbols indicate Luochuan (open diamonds), Chang'an (solid triangles), Changwu (open squares), Wugong (open triangles), Weinan (solid circles). Green dots show profile averages.

4.3 Soil organic carbon

Concerning C-cycle parameters, the best-calibrated rate constants (k) were found at: k_{HUM}=0.0025 yr^{-1} (figure 6.A) and k_{RPM} =0.02 yr^{-1} (figure 6.B). The found k_{HUM} and k_{RPM} were lower than the values reported by Todorovic et al. (2010), Stamati et al. (2013), Yu et al.

(2013), Finke et al. (2019), and the default RothC rates (see table 2), whereas k_{HUM} was within the range reported by Shirato et al. (2004) for Andosols.

The low k_{HUM} indicates a longer turnover period, and therefore soil can accumulate more soil organic matter. This is reasonable due to several reasons. In the CLP, the climate (arid to semi-humid) variables may be the most critical; low precipitation may reduce the organic matter decomposition rate. In contrast, it should be noted that the low precipitation could also limit vegetation growth and decrease plant litter supply. The found k_{HUM} may be a reasonable value for calcareous loess soils (Ca^{+2} rich, high pH) that can provide better protection to SOC. Several authors have found that soils rich in calcite can store more organic matter, thereby decreasing turnover rates (e.g. Rasmussen et al., 2018; Rowley et al., 2018). Via the low k_{HUM}, a SOC-protection process is mimicked and we assume that this k_{HUM} is reasonable for the soils of the CLP. Furthermore, silt-rich clayey fine-parent material can also provide better protection to SOC (e.g. Hassink, 1997; Stemmer et al., 2000), and dust deposition can bury fresh organic material, resulting in low SOC turnover rates. The low k_{RPM} suggests a relatively slow decomposition of RPM than that of the default RothC value (table 2), which was originally established for agricultural soils.

Table.2 Calibrated SOC cycle parameters from other studies and in this study and default values.

Reference	k_{HUM}	k_{RPM}	fr_{ecto}	Vegetation and study area
Stamati et al. (2013)	0.27 0.0041	0.34 0.21		Grassland, Lowa, USA Shrubland, Crete, Greece
Yu et al. (2013)	0.016-0.019 0.0065-0.0074	0.3 0.27	0.37-0.43 0.30-0.38	Forests, China Forests, Belgium
Todorovic et al.(2010)	0.009	0.6(fixed)		Cropland, Austria
Finke et al. (2019) (5 pool)	0.012	0.089		Grassland, California
Finke et al. (2019) (4 pool)	0.008	0.089		Grassland, California

In this study	0.0025	0.02	0.60	Grass/shrubs, forests, China
Default	0.02	0.3	0.58	

The calibrated fr_{ecto} in the grass/shrubs litter was 0.60 (figure 6.C), which was approximately similar to the SoilGen2 model default (0.58) based on measured data by Kononova (1975). The found ratio of ectorganic/endorganic litter (60/40) was similar to the default ratio (58/42) in SoilGen2. The partitioning coefficient CO_2 / (BIO+HUM) (figure 6.D) was higher (2.1) than the RothC default value (1.67). Possible reasons for this are (i) that the actual ratio varied with clay contents different from the ones used to calibrate the RothC26.3 model, and (ii) clay contents in SoilGen2 vary over time.

However, the calibrated carbon cycle parameters are conditional to the plant litter inputs; these were based on LOVECLIM simulated mean annual precipitation and temperature. Neither SoilGen2 nor RothC does determine climate-dependent vegetation growth (biomass production) and organic carbon input into the soil. We assumed root litter distribution according to a root density function, where plant roots depths decrease with soil depths per vegetation type.

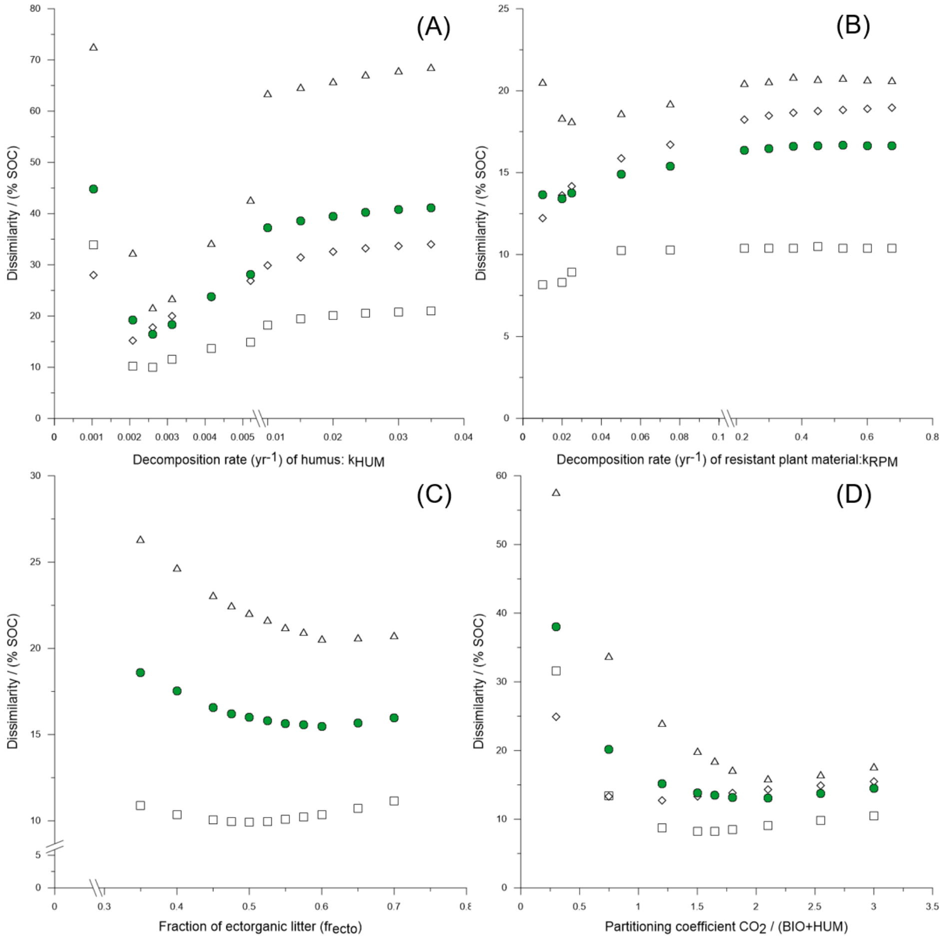

Figure 6. Dissimilarity (%) for different values of (A). $k_{HUM,}$ (B). k_{RPM} (C). fr_{ecto} in two profiles (D). the partitioning coefficient CO_2 / (BIO+HUM), in three profiles: Xifeng, Chenjiagou, Taoyu are denoted by triangles, diamonds, squares, respectively. Green dots show profile averages.

Table 3 presents all the best-calibrated results for the ten parameters.

Table 3. A summary of the calibrated parameters and best-calibrated values.

	Process parameter with units	Optimal value
(i)	Dissolution constant of calcite ($\log_{10} k_{so}$)	-9.0
(ii)	Interception evaporation fraction (-) for grass/shrubs/agriculture	0.03
(iii)	Thickness of the ectorganic layer (mm)	0.5
(iv)	Pressure head (hPa) at which macropores empty	-18
(v)	Filter coefficient for clay (-)	0.5
(vi)	Particle splitting probability and	2.163×10^{-6}
	soil temperature change °C / hour	0.95
(vii)	Decomposition rate (yr^{-1}) of humus	0.0025
(viii)	Ratio of ectorganic/endorganic litter (-)	60/40
(ix)	Decomposition rate of (yr^{-1}) of resistant plant material	0.02
(x)	Partitioning coefficient CO_2 / (BIO+HUM) (-)	2.1

4.4 Effect of dust deposition scenarios on the quality of the calibration result

Certainly, due to longer time scales of paleosol formation, soil-forming boundary conditions can be heavily affected by uncertainty. Little is known about the degree of uncertainty with respect to the calibrated soil profiles. If such boundary conditions are proven to be influential, this means that besides calibrating internal soil process parameters to simulate paleosol development, the uncertainty of model boundary conditions should also be considered. However, calibrating boundary conditions is unusual; it requires substantial computational effort as perturbations of time series of model boundary conditions must be evaluated (Minasny et al., 2015). The impact of ten reconstructed dust scenarios on the quality of the calibrations are shown in table 4 which gives the scaled dissimilarity results on a % scale.

Table 4. Impact of ten dust deposition rhythms on the quality of calibrations, expressed by standard deviations relative to the (scaled) dissimilarity of the calibration (Eq. 4).

Soil profiles	**Soil variables**			
	SOC	**CEC**	**Calcite**	**<2 µm fraction**
Taoyu	0.71%	0.01%	61.63%	3.99%
Xifeng	22.09%	0.40%	116.43%	0.18%
Chenjiagou	2.75%	0.08%	42.70%	1.87%
Average	8.52%	0.16%	73.59%	2.01%

As shown in table 4, the quality of simulated calcite contents responds strongly to the dust deposition scenarios, with an average standard deviation greater than 50%. It was to be expected that the highest uncertainty was obtained for calcite as the profile distribution of calcite is closely related to the input at the surface via dust and the interplay with subsequent leaching processes. In decreasing order of sensitivity to dust deposition rhythm, soil properties were ranked Calcite> soil organic carbon>2μm fraction>CEC. The CEC showed the smallest uncertainty, and 2μm fraction was also small because of lower clay migration in the Holocene soils.

Unexpectedly, the uncertainty of CEC is minute (table 4), however in the present study, the simulated CEC was largely overestimated in the top soils while usually underestimated in the subsoils (data not shown). This may have been caused by combined (in) accuracies of simulated SOC and 2μm fractions during simulations, as a relation between SOC and 2μm fraction is used to calculate the CEC in the SoilGen2 model. Thus, errors of SOC and clay content propagate into the CEC. Therefore, the (in) accuracy of simulated CEC can be affected partly by the dust deposition distribution over time and partly by inaccuracy of the assumed relation (Foth and Ellis (1996: p.57) between SOC, clay and CEC.

Figures 7, 8, 9 and 10 show the scaled dissimilarity variations compared to the final calibration results in each dust addition scenario for the above soil properties. Note that vertical axis-scales are different. In general, the comparison between the dust scenarios to the final calibrated results revealed that the calcite, organic carbon and CEC fluctuations were larger in Xifeng than in the other two sites (figures 7, 8 and 9); these are located south of Xifeng. An opposite trend was observed for simulated 2μm fraction (figure 10), where the fluctuations were relatively small in Xifeng. Note that clay content distribution was calibrated for MIS13 because clay migration in the Holocene is minor. Fluctuations in simulation quality must therefore entirely be attributed to the sediment properties. Our findings suggest that the impact of uncertain dust input rhythms varies between sites. The impact is larger for faster soil development processes (calcite redistribution, SOC-accumulation) and less for slower processes such as clay migration. Moreover, it is important to note that the uncertainty caused by variants of dust addition is larger than that of the calibrations (e.g. figure 8). It is worth mentioning that uncertainty of dust deposition rates can exist due to lack of dating of these Holocene soils and in paleosols. It has been emphasized that the different quantities of dust addition can contribute to uncertainty during formation of paleosols in the CLP (see review Meijer et al., 2020). However, it is impossible to assess the uncertainty of dust addition rates in the MIS13 paleosols in the present study since we only have two available geologic dust addition rhythms (Guo et al., 2009).

In summary, the dust deposition scenarios strongly affected the quality of the calibration. Thus, accuracy of dust scenarios should be considered during interglacial paleosol simulations.

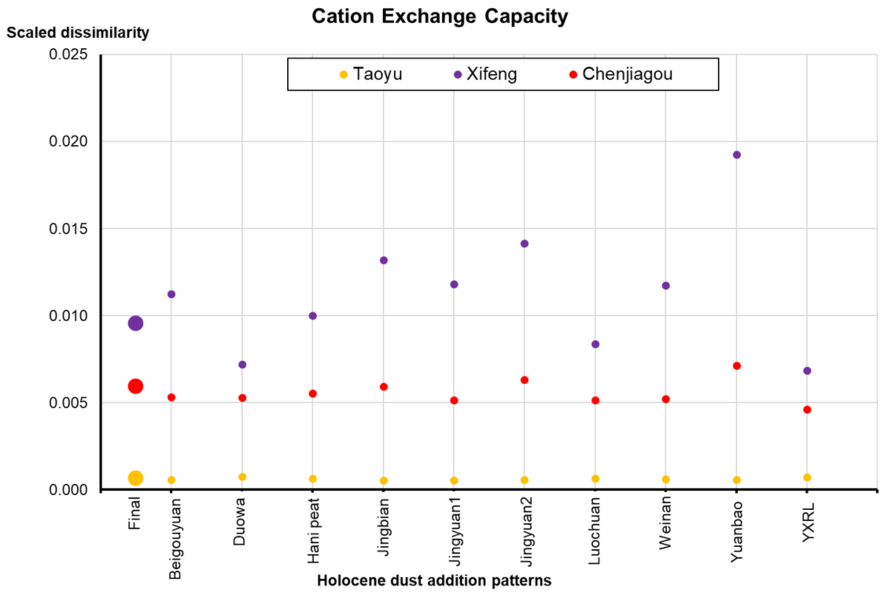

Figure 7. Scaled dissimilarity between dust scenarios (rightmost) and calibrated three Holocene sites (fat dots) for simulated CEC.

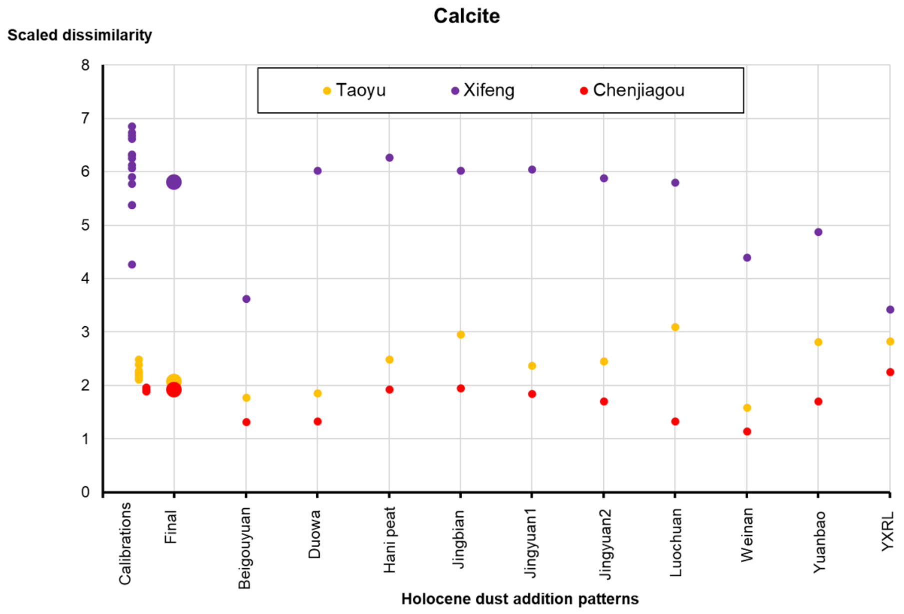

Figure 8. Scaled dissimilarity between dust scenarios (rightmost) and calibrated three Holocene sites (fat dots) and during calibrations (leftmost) for calcite content.

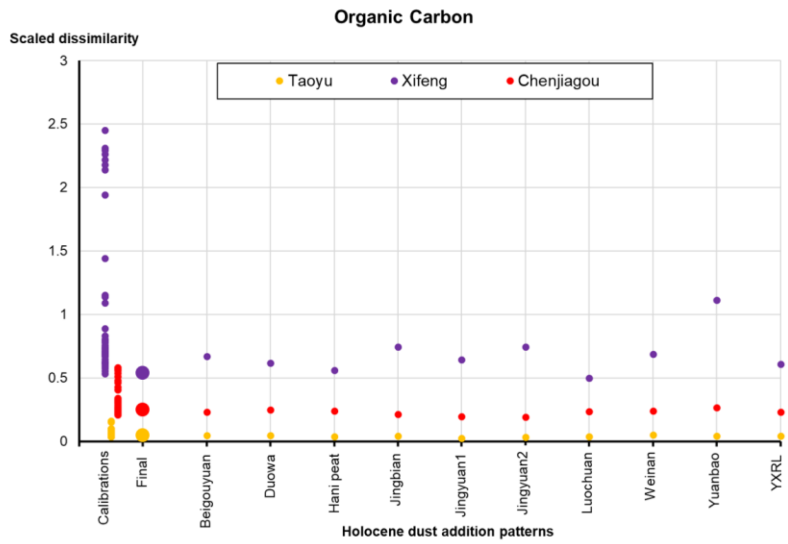

Figure 9. Scaled dissimilarity between dust scenarios (rightmost) and calibrated three Holocene sites (fat dots) and during calibrations (leftmost) for organic carbon.

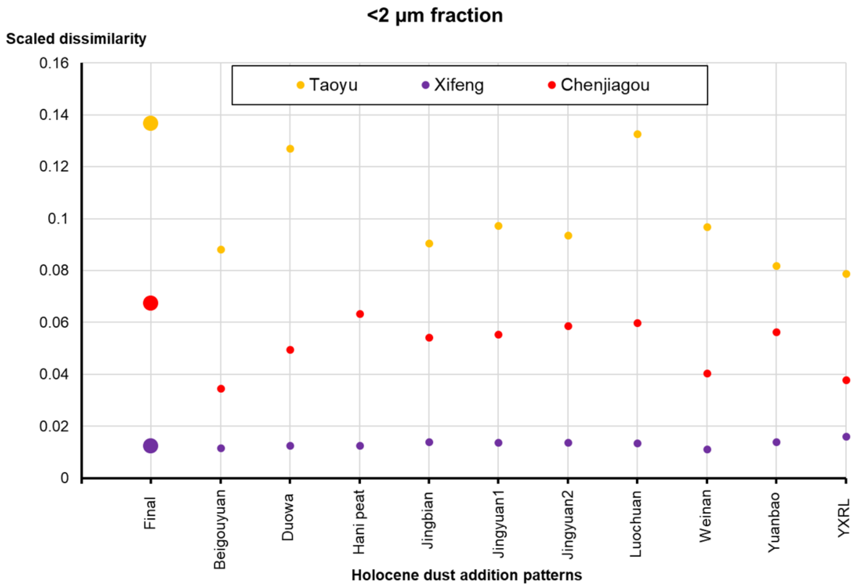

Figure 10. Scaled dissimilarity between dust scenarios (rightmost) and three Holocene sites (fat dots) for simulated 2µm fraction.

5. Conclusions:

The most sensitive soil-forming process parameters were calibrated in the SoilGen2 model for the CLP. An optimal value per parameter was found by confronting measurements to simulations and calculating the dissimilarity between both.

Our results show that: $\log_{10}k_{so}$=-9.0, the interception evaporation for grass/scrubs/agriculture= 3%, the filter coefficient (-)=0.5, PS_{max} and B=2.163x10^{-6} and 0.95 °C / hour, respectively, the ectorganic layer thickness =0.5 mm, the decay rates: k_{HUM}=0.0025 yr^{-1}, k_{RPM}=0.02 yr^{-1} and fraction of litter that is ectorganic=0.60 and partitioning coefficient CO_2 / (BIO+HUM)=2.1. These values fall inside previously found ranges. As an exception, the pressure head ($h\text{-}\theta_{macro}$) at which macropores empty did not respond to the calibration, which was attributed to the semi-arid climate. This leads to the conclusion that sensitivity analyses done in one climate may not be fully applicable to another climate.

Our results also show that SoilGen2-simulated/calibrated soil properties were highly sensitive to alternative Holocene dust deposition rhythms. The sensitivity varied in the following order: Calcite>soil organic carbon>2µm fraction>CEC by 73.59%, 8.52%, 2.01% and 0.16% respectively. The study shows that dust addition is an influential soil formation process in the CLP. Therefore, both the amount and rhythm of the dust deposition are important variables for quantifying paleosol development with process-based soil models in future studies. The uncertainty of process-based soil models with large run-time, like SoilGen2, would benefit from considering the accuracy of input data. In conclusion, our study emphasizes the equal importance of calibrating soil process parameters and defining correct external forcings in the future use of soil models.

Our results show that on the millennial time scale, uncertain model input and boundary conditions propagate through the model. As a result, even after calibrations, soil models are not free from these uncertainties. To increase the confidence in the calibrated model parameters, a model testing will be performed on an independently measured soil dataset in a future study.

Author contributions

Keerthika N. Ranathunga did the data curation, visualization, investigation and writing-original draft preparation and wrote the paper. Peter A. Finke conceptualized the experiment, provided the software, reviewed, co-wrote the paper and supervised the research. Qiuzhen Yin provided resources, funding acquisition and reviewed the paper and supervised the research. Yanyan Yu provided resources, funding acquisition and reviewed the paper.

Declaration of competing interests

The authors declare that they have no known competing financial interests or personal relationships that could have appeared to influence the work reported in this paper.

Data availability

The authors confirm that the data supporting the findings of this study are available within the article and its supplementary materials.

Acknowledgements

This work and K.N. Ranathunga are supported by the Fonds de la Recherche Scientifique FNRS (F.R.S.-FNRS) under grant MIS F.4529.18. Y.Y. Yu acknowledges the National Natural Science Foundation of China (no. 41877441) for supporting her research. Q.Z. Yin is Research Associate F.R.S.-FNRS. We are grateful to Dr. Hao Lu for his assistance in modifying the map of the CLP of this manuscript.

References

Albani, S., Mahowald, N.M., Winckler, G., Anderson, R.F., Bradtmiller, L.I., Delmonte, B., François, R., Goman, M., Heavens, N.G., Hesse, P.P., Hovan, S.A., Kang, S.G., Kohfeld, K.E., Lu, H., Maggi, V., Mason, J.A., Mayewski, P.A., McGee, D., Miao, X., Otto-Bliesner, B.L., Perry, A.T., Pourmand, A., Roberts, H.M., Rosenbloom, N., Stevens, T., Sun, J., 2015. Twelve thousand years of dust: The Holocene global dust cycle constrained by natural archives. Climate of the Past 11, 869–903. doi:10.5194/cp-11-869-2015

An, Z.S., Liu, T., Zhou, Y., Sun, F., Ding, Z., 1987. The paleosol complex S5 in the China Loess Plateau - A record of climatic optimum during the last 1.2 Ma. GeoJournal 15, 141–143. doi:10.1007/BF00157939

An, Z.S., Kukla, G., Porter, S.C., Xiao, J. Le, 1991. Late quaternary dust flow on the chinese Loess Plateau. Catena 18, 125–132. doi:10.1016/0341-8162(91)90012-M

Carlyle-Moses, D.E., Gash, J.H.C., 2011. Rainfall interception loss by forest canopies. In: Levia, D.., Carlyle-Moses, D.., Tanaka, T. (Eds.), Forest Hydrology and Biogeochemistry, Synthesis of Past Research and Future Directions. Springer Inc, Dordrecht, pp. 407–423. doi:10.1007/978-94-007-1363-5

Coleman, K., Jenkinson, D.S., 2014. RothC-26.3 - A Model for the turnover of carbon in soil. Model Description and Windows Users Guide (November 1999 issue (modified June 2014). Harpenden,UK. doi:10.1007/978-3-642-61094-3_17

Crockford, R.H., Richardson, D.P., 2000. Partitioning of rainfall into throughfall, stemslow and interception effect of forest type, ground cover and climate. Hydrological Processes 14, 2903–2920. doi:10.1002/1099-1085(200011/12)14:16/17<2903::AID-HYP126>3.0.CO;2-6

DeNovio, N.M., Saiers, J.E., Ryan, J.N., 2004. Colloid Movement in Unsaturated Porous Media: Recent Advances and Future Directions. Vadose Zone Journal 3, 338–351. doi:10.2136/vzj2004.0338

Finke, P., Opolot, E., Balesdent, J., Berhe, A.A., Boeckx, P., Cornu, S., Harden, J., Hatté, C., Williams, E., Doetterl, S., 2019. Can SOC modelling be improved by accounting for pedogenesis? Geoderma 338, 513–524. doi:10.1016/j.geoderma.2018.10.018

Finke, P.A., 2012. Modeling the genesis of luvisols as a function of topographic position in loess parent material. Quaternary International 265, 3–17. doi:10.1016/j.quaint.2011.10.016

Finke, P.A., 2020. SOILGEN: A simulation model for soil development in various parent materials. Dept. Environment, Ghent, Belgium.

Finke, P.A., Hutson, J.L., 2008. Modelling soil genesis in calcareous loess. Geoderma 145, 462–479. doi:10.1016/j.geoderma.2008.01.017

Finke, P.A., Samouëlian, A., Suarez-Bonnet, M., Laroche, B., Cornu, S.S., 2015. Assessing the usage potential of SoilGen2 to predict clay translocation under forest and agricultural land uses. European Journal of Soil Science 66, 194–205. doi:10.1111/ejss.12190

Finke, P.A., Yin, Q.Z., Bernardini, N.J., Yu, Y., 2017. Climate-soil model reveals causes of differences between Marine Isotope Stage 5e and 13 paleosols. Geology 46, 99–102. doi:10.1130/G39301.1

Finke, P.A., Ranathunga Arachchige, K.N., Verdoodt, A., Yu, Y.Y., Yin, Q.Z., 2021. Unraveling loess records of climate change from the Chinese loess plateau using process-based models. In: Hunt, A., Egli, M., Faybishenko, B. (Eds.), Hydrogeology, Chemical Weathering and Soil Formation. AGU Geophysical Monograph Series, pp. 163–175. doi:10.1002/9781119563952.ch8

Foth, H.D., Ellis, B.G., 1996. Soil Fertility, second edi. ed. CRC press, Lewis. doi:https://doi.org/10.1201/9780203739341

Geißler, C., Kühn, P., Böhnke, M., Bruelheide, H., Shi, X., Scholten, T., 2012. Splash erosion potential under tree canopies in subtropical SE China. Catena 91, 85–93. doi:10.1016/j.catena.2010.10.009

Gower, J.C., 1971. A General Coefficient of Similarity and Some of Its Properties. Biometrics 27, 857–871. doi:10.2307/2528823

Guo, Z.T., Ruddiman, W.F., Hao, Q.Z., Wu, H.B., Qiao, Y.S., Zhu, R.X., Peng, S.Z., Wel, J.J., Yuan, B.Y., Llu, T.S., 2002. Onset of Asian desertification by 22 Myr ago inferred from loess deposits in China. Nature 416, 159–163. doi:10.1038/416159a

Guo, Z.T., Berger, A., Yin, Q.Z., Qin, L., 2009. Strong asymmetry of hemispheric climates during MIS-13 inferred from correlating China loess and Antarctica ice records. Climate of the Past 5, 21–31. doi:10.5194/cp-5-21-2009

Hassink, J., 1997. The capacity of soils to preserve organic C and N by their association with clay and silt particles. Plant and Soil 191, 77–87. doi:10.1023/A:1004213929699

Hao, Q., Guo, Z., 2005. Spatial variations of magnetic susceptibility of Chinese loess for the last 600 kyr: Implications for monsoon evolution. J. Geophys. Res. Solid Earth 110, 1–10. https://doi.org/10.1029/2005JB003765

Hörmann, G., Branding, A., Clemen, T., Herbst, M., Hinrichs, A., Thamm, F., 1996. Calculation and simulation of wind controlled canopy interception of a beech forest in Northern Germany. Agricultural and Forest Meteorology 79, 131–148. doi:10.1016/0168-1923(95)02275-9

Huang, C.C., Pang, J., Chen, S., Zhang, Z., 2003. Holocene dust accumulation and the formation of polycyclic cinnamon soils (luvisols) in the Chinese Loess Plateau. Earth Surface Processes and Landforms 28, 1259–1270. doi:10.1002/esp.512

Hutson, J.L., Wagenet, R.J., 1992. LEACHM: Leaching, Estimation and Chemistry Model : a Process-based Model of Water and Solute Movement, Transformations, Plant Uptake and Chemical Reactions in the Unsaturated Zone, Continuum Vol.2, Version 3 (Water Resources Institute). Department of Agronomy, Cornell University, Ithaca, NY.

Jacobson, R.L., Langmuir, D., 1974. Dissociation constants of calcite and CaHC03+ from 0 to 50°C. Geochimica et Cosmochimica Acta 38, 301–318. doi:10.1016/0016-7037(74)90112-4

Jarvis, N.J., Villholth, K.G., Ulén, B., 1999. Modelling particle mobilization and leaching in macroporous soil. European Journal of Soil Science 50, 621–632. doi:10.1046/j.1365-2389.1999.00269.x

Jenny, H., 1941. Factors of Soil Formation. A System of Quantitative Pedology. McGraw-Hill Book Company, New York, London.

Jian, S., Zhao, C., Fang, S., Yu, K., 2015. Effects of different vegetation restoration on soil water storage and water balance in the Chinese Loess Plateau. Agricultural and Forest Meteorology 206, 85–96. doi:10.1016/j.agrformet.2015.03.009

Kemp, R.A., 2001. Pedogenic modification of loess: Significance for palaeoclimatic reconstructions. Earth-Science Reviews 54, 145–156. doi:10.1016/S0012-8252(01)00045-9

Keyvanshokouhi, S., Cornu, S., Samouëlian, A., Finke, P., 2016. Evaluating SoilGen2 as a tool for projecting soil evolution induced by global change. Science of the Total Environment 571, 110–123. doi:10.1016/j.scitotenv.2016.07.119

Klaassen, W., Bosveld, F., Water, E. De, 1998. Water storage and evaporation as constituents of rainfall interception. Journal of Hydrology 212–213, 36–50. doi:10.1016/S0022-1694(98)00200-5

Kohfeld, K.E., Harrison, S.P., 2003. Glacial-interglacial changes in dust deposition on the Chinese Loess Plateau. Quaternary Science Reviews 22, 1859–1878. doi:10.1016/S0277-3791(03)00166-5

Kononova, M.M., 1975. Humus of Virgin and Cultivated Soils. In: Gieseking, J.E. (Ed.), Soil Components: Vol. 1: Organic Components. Springer Berlin Heidelberg, pp. 475–526. doi:10.1007/978-3-642-65915-7_8

Kukla, G., An, Z., 1989. Loess stratigraphy in Central China. Palaeogeography, Palaeoclimatology, Palaeoecology 72, 203–225. doi:10.1016/0031-0182(89)90143-0

Kuzyakov, Y., Zamanian, K., 2019. Reviews and syntheses: Agropedogenesis-Humankind as the sixth soil-forming factor and attractors of agricultural soil degradation. Biogeosciences 16, 4783–4803. doi:10.5194/bg-16-4783-2019

Li, G., Chen, J., Chen, Y., 2013. Primary and secondary carbonate in Chinese loess discriminated by trace element composition. Geochimica et Cosmochimica Acta 103, 26–35. doi:10.1016/j.gca.2012.10.049

Li, J., Song, Z., Ruan, L., Yang, L., Zwieten, L. Van, Hu, Z., He, S., Chenwu, W., Wang, H., 2019. The contribution of Asian dust in the pedogenesis of ultisols in Southeastern China determined by soil grain size. Journal of Soils and Sediments 19, 232–240. doi:10.1007/s11368-018-2012-5

Li, X., Xiao, Q., Niu, J., Dymond, S., Doorn, N.S. van, Yu, X., Xie, B., Lv, X., Zhang, K., Li, J., 2016. Process-based rainfall interception by small trees in Northern China: The effect of rainfall traits and crown structure characteristics. Agricultural and Forest Meteorology 218–219, 65–73. doi:10.1016/j.agrformet.2015.11.017

Li, Y., Zhang, W., Aydin, A., Deng, X., 2018. Formation of calcareous nodules in loess–paleosol sequences: Reviews of existing models with a proposed new “per evapotranspiration model.” Journal of Asian Earth Sciences 154, 8–16. doi:10.1016/j.jseaes.2017.12.002

Li, Y.Y., Shao, M.A., 2006. Change of soil physical properties under long-term natural vegetation restoration in the Loess Plateau of China. Journal of Arid Environments 64, 77–96. doi:10.1016/j.jaridenv.2005.04.005

Liu, T.., 1985. Loess and the Environment. China Ocean Press, Beijing.

Liu, W., Fox, J.E.D., Xu, Z., 2003. Nutrient budget of a montane evergreen broad-leaved forest at Ailao Mountain National Nature Reserve, Yunnan, southwest China. Hydrological Processes 17, 1119–1134. doi:10.1002/hyp.1184

Lu, H., Jia, J., Wang, Y., Yin, Q., Xia, D., 2018. The cause of extremely high magnetic susceptibility of the S5S1 paleosol in the central Chinese Loess Plateau. Quaternary International 493, 252–257. doi:10.1016/j.quaint.2018.05.046

Maher, B.A., 2016. Palaeoclimatic records of the loess/palaeosol sequences of the Chinese Loess Plateau. Quaternary Science Reviews 154, 23–84. doi:10.1016/j.quascirev.2016.08.004

Meijer, N., Dupont-Nivet, G., Licht, A., Trabucho-Alexandre, J., Bourquin, S., Abels, H.A., 2020. Identifying eolian dust in the geological record. Earth-Science Reviews 211. doi:10.1016/j.earscirev.2020.103410

Minasny, B., Finke, P., Stockmann, U., Vanwalleghem, T., McBratney, A.B., 2015. Resolving the integral connection between pedogenesis and landscape evolution. Earth-Science Reviews 150, 102–120. doi:10.1016/j.earscirev.2015.07.004

Morris, M.D., 1991. Factorial sampling plans for preliminary computational experiments. Technometrics 33, 161–174. doi:10.1080/00401706.1991.10484804

Nisbet, T.R., 2005. Water Use by Trees. Forestry Commission Information. 65 1–8.

Ochoa-Sánchez, A., Crespo, P., Célleri, R., 2018. Quantification of rainfall interception in the high Andean tussock grasslands. Ecohydrology 11, 1–11. doi:10.1002/eco.1946

Opolot, E., Yu, Y.Y., Finke, P.A., 2015. Modeling soil genesis at pedon and landscape scales: Achievements and problems. Quaternary International 376, 34–46. doi:10.1016/j.quaint.2014.02.017

Pang, J.L., Huang, C.C., 2006. Mid-Holocene soil formation and the impact of dust input in the middle reaches of the Yellow River, Northern China 171, 552–563. doi:10.1097/01.ss.0000228040.65023.1b

Porter, S.C., 2001. Chinese loess record of monsoon clinate during the last glacial-interglacial cycle. Earth-Science Reviews 54, 115–128. doi:10.1016/S0012-8252(01)00043-5

Rasmussen, C., Heckman, K., Wieder, W.R., Keiluweit, M., Lawrence, C.R., Berhe, A.A., Blankinship, J.C., Crow, S.E., Druhan, J.L., Hicks Pries, C.E., Marin-Spiotta, E., Plante, A.F., Schädel, C., Schimel, J.P., Sierra, C.A., Thompson, A., Wagai, R., 2018. Beyond clay: towards an improved set of variables for predicting soil organic matter content. Biogeochemistry 137, 297–306. doi:10.1007/s10533-018-0424-3

Rowley, M.C., Grand, S., Verrecchia, É.P., 2018. Calcium-mediated stabilisation of soil organic carbon. Biogeochemistry 137, 27–49. doi:10.1007/s10533-017-0410-1

Rutter, A.J., Morton, A.J., Robins, P.C., 1975. A Predictive Model of Rainfall Interception in Forests. II. Generalization of the Model and Comparison with Observations in Some Coniferous and Hardwood Stands. The Journal of Applied Ecology 12, 367–380. doi:10.2307/2401739

Sauer, D., Finke, P., Sørensen, R., Sperstad, R., Schülli-Maurer, I., Høeg, H., Stahr, K., 2012. Testing a soil development model against southern Norway soil chronosequences. Quaternary International 265, 18–31. doi:10.1016/j.quaint.2011.12.018

Savenije, H.H.G., 2004. The importance of interception and why we should delete the term evapotranspiration from our vocabulary. Hydrological Processes 18, 1507–1511. doi:10.1002/hyp.5563

Schaetzl, R.., Thompson, M.., 2015. Soils. soils genesis and geomorphology, 2nd ed. Cambridge university press.

Sheng, H., Cai, T., 2019. Influence of rainfall on canopy interception in mixed Broad-Leaved-Korean pine forest in Xiaoxing'an Mountains, northeastern China. Forests 10, 1–11. doi:10.3390/f10030248

Shirato, Y., Hakamata, T., Taniyama, I., 2004. Modified rothamsted carbon model for andosols and its validation: changing humus decomposition rate constant with pyrophosphate-extractable Al. Soil Science and Plant Nutrition 50, 149–158. doi:10.1080/00380768.2004.10408463

Stamati, F.E., Nikolaidis, N.P., Schnoor, J.L., 2013. Modeling topsoil carbon sequestration in two contrasting crop production to set-aside conversions with RothC - Calibration issues and uncertainty analysis. Agriculture, Ecosystems and Environment 165, 190–200. doi:10.1016/j.agee.2012.11.010

Stemmer, M., Roth, K., Kandeler, E., 2000. Carbon mineralization and microbial activity in a field site trial used for 14C turnover experiments over a period of 30 years. Biology and Fertility of Soils 31, 294–302. doi:10.1007/s003740050659

Stockmann, U., 2011. Quantifying pedogenesis processes.PHD thesis. The University of Sydney, New South Wales, Australia.

Su, L., Zhao, C., Xu, W., Xie, Z., 2016. Modelling interception loss using the revised Gash model: a case study in a mixed evergreen and deciduous broadleaved forest in China. Ecohydrology 9, 1580–1589. doi:10.1002/eco.1749

Sun, A., Guo, Z., Wu, H., Li, Q., Yu, Y., Luo, Y., Jiang, W., Li, X., 2017. Reconstruction of the vegetation distribution of different topographic units of the Chinese Loess Plateau during the Holocene. Quaternary Science Reviews 173, 236–247. doi:10.1016/j.quascirev.2017.08.006

Sun, Y., Wang, X., Liu, Q., Clemens, S.C., 2010. Impacts of post-depositional processes on rapid monsoon signals recorded by the last glacial loess deposits of northern China. Earth and Planetary Science Letters 289, 171–179. doi:10.1016/j.epsl.2009.10.038

Todorovic, G.R., Stemmer, M., Tatzber, M., Katzlberger, C., Spiegel, H., Zehetner, F., Gerzabek, M.H., 2010. Soil-carbon turnover under different crop management: Evaluation of RothC-model predictions under Pannonian climate conditions. Journal of Plant Nutrition and Soil Science 173, 662–670. doi:10.1002/jpln.200800311

VanBreemen, N., Buurman, P., 2002. Soil formation, 2nd ed, Journal of Chemical Information and Modeling. Springer Netherlands. doi:10.1007/0-306-48163-4

Vidic, N.J., Lobnik, F., 1997. Rates of soil development of the chronosequence in the Ljubljana Basin, Slovenia. Geoderma 76, 35–64. doi:10.1016/S0016-7061(96)00098-5

Wang, L., Wang, S.P., Shao, H.B., Wu, Y.J., Wang, Q.J., 2012. Simulated water balance of forest and farmland in the hill and gully region of the loess plateau in China. Plant Biosystems 146, 226–243. doi:10.1080/11263504.2012.709198

Wei, X., Liu, S., Zhou, G., Wang, C., 2005. Hydrological processes in major types of Chinese forest. Hydrological Processes 19, 63–75. doi:10.1002/hyp.5777

Yin, Q.Z., Berger, A., 2015. Interglacial analogues of the Holocene and its natural near future. Quaternary Science Reviews 120, 28–46. doi:10.1016/j.quascirev.2015.04.008

Yin, Q.Z., Guo, Z.T., 2008. Strong summer monsoon during the cool MIS-13. Climate of the Past, European Geosciences Union (EGU) 4, 29–34. doi:10.5194/cp-4-29-2008

Yu, Y., Wu, H., Finke, P.A., Guo, Z., 2016. Spatial and temporal changes of prehistoric human land use in the Wei River valley, northern China. Holocene 26, 1788–1801. doi:10.1177/0959683616645943

Yu, Y.Y., Finke, P.A., Wu, H.B., Guo, Z.T., 2013. Sensitivity analysis and calibration of a soil carbon model (SoilGen2) in two contrasting loess forest soils. Geoscientific Model Development 6, 29–44. doi:10.5194/gmd-6-29-2013

Zhang, G., Zeng, G.M., Jiang, Y.M., Huang, G.H., Li, J.B., Yao, J.M., Tan, W., Xiang, R., Zhang, X.L., 2006. Modelling and measurement of two-layer-canopy interception losses in a subtropical evergreen forest of central-south China. Hydrology and Earth System Sciences 10, 65–77. doi:10.5194/hess-10-65-2006

Zhou, J., Fu, B., Gao, G., Lü, Y., Liu, Y., Lü, N., Wang, S., 2016. Effects of precipitation and restoration vegetation on soil erosion in a semi-arid environment in the Loess Plateau, China. Catena 137, 1–11. doi:10.1016/j.catena.2015.08.015

Zwertvaegher, A., Finke, P., Smedt, P. De, Gelorini, V., Meirvenne, M. Van, Bats, M., Reu, J. De, Antrop, M., Bourgeois, J., Maeyer, P. De, Verniers, J., Crombé, P., 2013. Spatio-temporal modeling of soil characteristics for soilscape reconstruction. Geoderma 207–208, 166–179. doi:10.1016/j.geoderma.2013.05.013